Naval Research Laboratory
Washington, DC 20375-5320

Lithium-Ion Battery Failure: Effects of State of Charge and Packing Configuration

Neil S. Spinner

National Research Council Postdoctoral Associate
Navy Technology Center for Safety and Survivability
Chemistry Division

Katherine M. Hinnant
Steven G. Tuttle
Susan L. Rose-Pehrsson

Navy Technology Center for Safety and Survivability
Chemistry Division

August 22, 2016

REPORT DOCUMENTATION PAGE

1. REPORT DATE (DD-MM-YYYY)
22-08-2016

2. REPORT TYPE
Memorandum Report

3. DATES COVERED (From - To)
January 2014 – January 2016

4. TITLE AND SUBTITLE

Lithium-Ion Battery Failure: Effects of State of Charge and Packing Configuration

5a. CONTRACT NUMBER
N0001414WR20004

5b. GRANT NUMBER

5c. PROGRAM ELEMENT NUMBER

6. AUTHOR(S)

Neil S. Spinner,* Katherine M. Hinnant, Steven G. Tuttle, and Susan L. Rose-Pehrsson

5d. PROJECT NUMBER

5e. TASK NUMBER

5f. WORK UNIT NUMBER
61-9496-04

7. PERFORMING ORGANIZATION NAME(S) AND ADDRESS(ES)

Naval Research Laboratory
4555 Overlook Avenue, SW
Washington, DC 20375-5320

8. PERFORMING ORGANIZATION REPORT NUMBER

NRL/MR/6180--16-9689

9. SPONSORING / MONITORING AGENCY NAME(S) AND ADDRESS(ES)

Office of Naval Research
One Liberty Center
875 N. Randolph St., Suite 1425
Arlington, Virginia 22203-1995

10. SPONSOR / MONITOR'S ACRONYM(S)

ONR 6.2

11. SPONSOR / MONITOR'S REPORT NUMBER(S)

12. DISTRIBUTION / AVAILABILITY STATEMENT

Approved for public release; distribution is unlimited.

13. SUPPLEMENTARY NOTES
*National Research Council Postdoctoral Associate

14. ABSTRACT

Lithium-ion battery safety remains a significant concern, as battery failure leads to ejection of hazardous materials and rapid heat release that can potentially cause propagation from cell to cell resulting in a total catastrophic failure event. Development of effective mitigation strategies necessitates the controlled study of battery failure events to build a database and improve understanding of important characteristics relating to safety, such as heat release, hazardous materials ejection, and thermal propagation. The U.S. Naval Research Laboratory (NRL) has been conducting a myriad of these battery failure experiments for several years, investigating a variety of different battery chemistries, geometries, abuse scenarios, and analysis techniques. In this report, different states of charge and packing configurations of a commercially available 18650 lithium-ion battery are studied to determine their impact on heat propagation, internal battery temperatures, radial temperature distributions, and failure characteristics. Internal temperatures were obtained by designing and fabricating 18650 surrogate cells with embedded thermocouples which contained no active materials and were reused for multiple failure tests.

15. SUBJECT TERMS

Lithium-ion cell	Battery state of charge
Lithium-ion battery fire	Packing configuration

16. SECURITY CLASSIFICATION OF:

a. REPORT	b. ABSTRACT	c. THIS PAGE
Unclassified Unlimited	Unclassified Unlimited	Unclassified Unlimited

17. LIMITATION OF ABSTRACT
Unclassified Unlimited

18. NUMBER OF PAGES
20

19a. NAME OF RESPONSIBLE PERSON
Steven G. Tuttle

19b. TELEPHONE NUMBER (include area code)
(202) 404-3419

Standard Form 298 (Rev. 8-98)
Prescribed by ANSI Std. Z39.18

i

Contents

1.0 Background and Motivation

Lithium-ion batteries are a popular choice of power source for a variety of military systems due to their promise of high power and high energy density. However, safety remains a significant concern, as battery failure leads to ejection of hazardous materials and rapid heat release that can potentially cause propagation from cell-to-cell resulting in a total catastrophic failure event. These types of concerns can often present large obstacles for obtaining approval to implement new systems or upgrade existing power sources with more effective, state-of-the-art lithium-ion battery packs. Gaining approval for these systems hinges on the assurance of safe operation and, in the event of battery failure, effective mitigation and/or evacuation strategies (for the hazardous batteries, nearby personnel, or both) to prevent injury or loss of life.

Development of such strategies necessitates the controlled study of battery failure events to build a database and improve understanding of important characteristics relating to safety, such as heat release, hazardous materials ejection, and thermal propagation. The US Naval Research Laboratory (NRL) has been conducting a myriad of these battery failure experiments for several years, investigating a variety of different battery chemistries, geometries, abuse scenarios, and analysis techniques [1-18]. However, despite the cache of data present in these reports, much still remains to be elucidated, specifically concerning the effects of state of charge (SOC) and multi-cell packing configuration on cell-to-cell failure propagation, particularly with respect to radial temperature distributions and internal temperature rise.

Battery failure can be initiated via a number of different abuse scenarios, such as overheating, overcharging, puncture/crushing, water immersion, or short circuiting. Consequently, under each of these situations the failing battery may exist at virtually any SOC, making it crucial to be able to gauge the level of threat as a function of SOC. Unfortunately, the importance of SOC on battery failure has been only minimally studied within the scope of both NRL reports [4,6,15] and the general literature [19-22], and lacking from many of these reports are thermal and quantitative analyses in addition to qualitative observations of failure events. Thus, a more thorough analysis of SOC effects on lithium-ion battery failure, particularly in multi-cell packs, is needed.

In addition to SOC, multi-cell packing configurations can highly influence lithium-ion battery failure events, especially with regard to cell-to-cell propagation. We have previously begun preliminary investigations of differences between hexagonal and rectangular geometric packings of 18650 cylindrical cells via computational modeling, comparing the rate of energy release and thermal propagation during failure events [17]. One of the key discoveries from these simulations was that energy propagation during failure likely occurs primarily in the vertical direction, as opposed to laterally, due to directed venting of hot materials and as a result of buoyancy-driven flow of ambient air surrounding the battery pack. This suggests that the cells most in danger of being impacted are those directly above, rather than adjacent to, a failing battery, meaning cell-to-cell failure propagation may be more likely to occur vertically as opposed to horizontally.

Another relevant point of emphasis with respect to cell packings concerns anisotropy of the 18650 battery's thermal conductivity; that is, due to the internal construction of a cylindrical cell, heat transfer in the axial direction is much more facile than in the radial direction [23-25]. This can give rise to either moderate radial temperature distributions ($< 10°C$) during normal cell operation [26], or more extreme discrepancies between surface and internal temperatures (as high as 40-50°C) during an adjacent failure or rapid heating event [27-29]. With respect to this anisotropy, a related area of study that has not been investigated is the effect of horizontal and vertical cell packings on these radial temperature distributions. One would expect more dramatic radial temperature discrepancies for a horizontal package of cells since heat transfer occurs in the radial direction, compared with a vertical package where heat transfer propagates axially to nearby cells either above or below the failing cell.

In this report, different SOCs and packing configurations of a commercially-available 18650 lithium-ion battery are studied to determine their impact on heat propagation, internal battery temperatures, radial temperature distributions, and failure characteristics. Internal temperatures were obtained by designing and fabricating 18650 surrogate cells with embedded thermocouples which contained no active materials and were reused for multiple failure tests.

2.0 Experimental

Failure tests were carried out using a 5 m³ two-man decompression chamber that has been re-purposed as an environmental test chamber. Numerous modifications have been made to enable remote control and monitoring of equipment and chamber functions, details of which can be found in our previous publications [16,18]. Failure tests were conducted inside the chamber using a myriad of instrumentation and devices, which are described in detail in our published works [16,18] and are also summarized in Table 1. The active batteries used in all tests were commercially-available 18650 $LiCoO_2$ lithium-ion batteries (Tenergy Corporation, 3.7V, 2.6Ah rated), and all failure events were initiated via overheating.

Two different packing configurations of 18650 cells were assembled: horizontal and vertical. Labeled diagrams for both configurations are shown in Figure 1. In each setup, only one active lithium-ion battery was used, and surrogate 18650 cells with no active materials were used to fill in the packings. Figure 2 shows a photograph and labeled diagram of the surrogate cells fabricated for these tests, which consisted of alternating layers of mica (ultra high temperature, 0.61 mm thick) and stainless steel shim (0.051 mm thick, 51 mm width) rolled into a cylinder and inserted into an empty 18650 cell casing (details regarding the thermophysical properties and failure event performance of these novel surrogate cells have been submitted for publication [30]). K-type thermocouples (Omega) were affixed to three locations on the "jelly roll"-type surrogate cell design: one in the center and two radially spaced on opposite ends but still contained entirely inside the cell casing. Small holes were punched in the bottom of the casing to allow thermocouple wires to pass through. Once all materials were inside the cell casing, the cell was grooved (MSK-
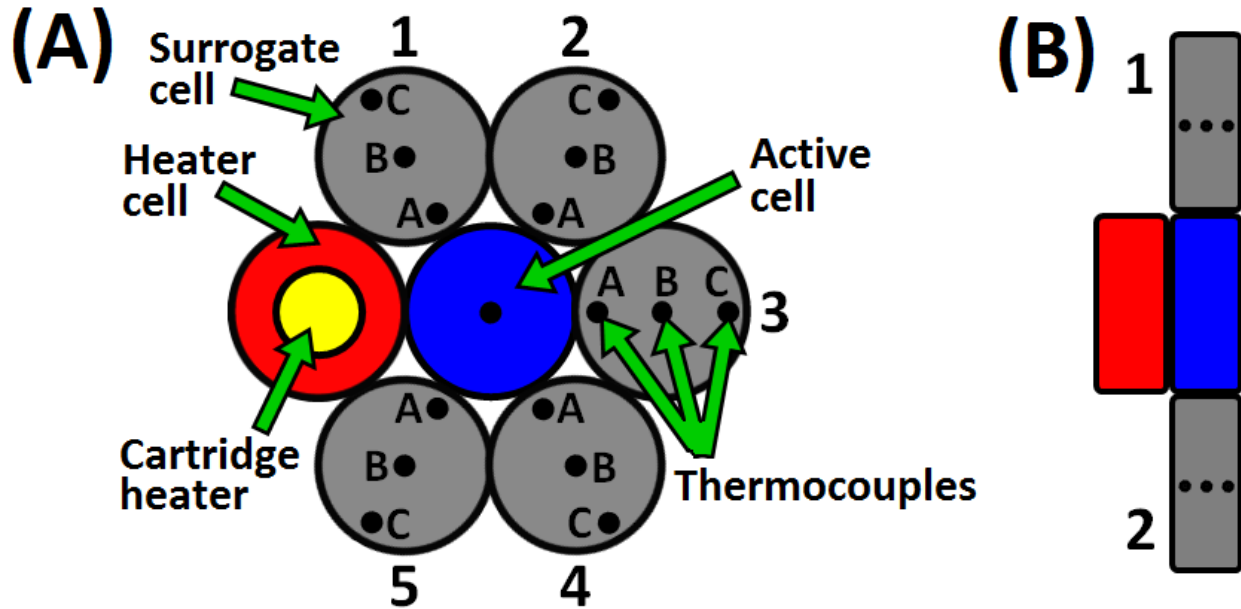
Figure 1. Labeled diagrams of (A) hexagonal and (B) vertical arrangements of 18650 active (blue), surrogate (gray) and heater (red/yellow) cells, as well as thermocouple locations (black dots).

500 Semi-Auto Grooving Machine, MTI Corp.), a cap was added on top, and it was crimped shut (MSK-510M Hydraulic Crimping Machine, MTI Corp.).

    For overheating batteries to the point of failure, a separate 18650 surrogate heater cell was created consisting of an aluminum core with an embedded cartridge heater, which was then connected to a variable autotransformer to modulate the heat output. In all failure tests, the heater cell was positioned directly adjacent to the active cell (see Fig. 1) to effectively initiate overheat failure events. In addition to the two packing configurations, three different SOCs were
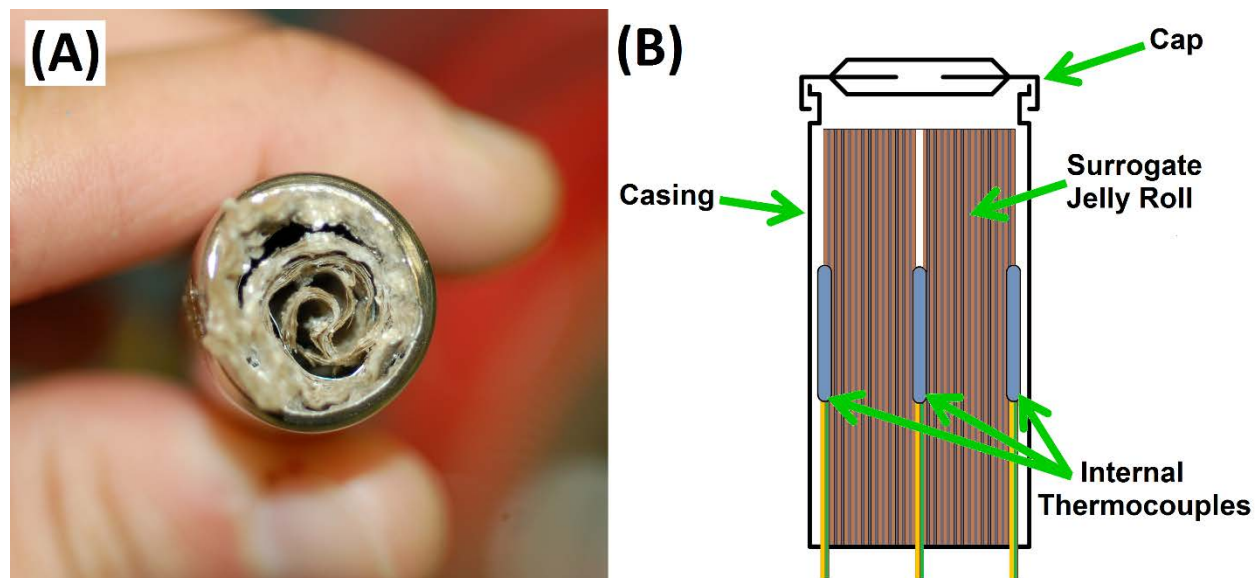
Figure 2. (A) Photograph and (B) labeled schematic of custom 18650 surrogate cell.

3

investigated: 30%, 100%, and severely overcharged. For the 30% tests, active cells were used as-received from the manufacturer. Charging to 100% was performed by applying a current of 200 mA until the upper cutoff voltage of 4.2V was reached, followed by holding at 4.2V until the current dropped to below 52 mA, using a Model 263A Potentiostat/Galvanostat (Princeton Applied Research). Severe overcharging was carried out using an 18V-10A power supply (Sorensen XPH Series) until an internal safety feature of the active cell tripped (typically when voltage reached >5V) and the battery went to open circuit.

Table 1. Summary of devices and instrumentation used in all tests.

Instrument/Device	Specifications	Short Name	Manufacturer	Purpose
Compact Reconfigurable Embedded Control and Acquisition Systems	cRIO-9014, cRIO-9025	CompactRIO	National Instruments	Remote control and monitoring of chamber functions, temperature data
LabVIEW Software	---	LabVIEW	National Instruments	Control and programming of remote functions
High Speed Cameras	HiSpec1	HS	Fastec Imaging	Battery failure videos
Camera Zoom Lenses	Nikkor f/2.8D 28mm, Nikkor f/1.2 50mm	---	Nikon	Battery failure videos
Infrared Cameras	A300, SC6800	IR	FLIR Systems	Battery failure videos
ZnSe Window	50mm dia. x 2mm thick, 3-12μm coating	---	Edmund Optics	IR camera enclosure
Variable Transformer	3PN1010B, 140V 10A	---	Staco Energy Products Co.	Modulating cartridge heater
Power Supply	Sorensen XPH Series, 18V 10A	---	AMETEK Inc.	Overcharging battery

3.0 Results and Discussion

3.1 Horizontal Packing

A hexagonal arrangement of cells was constructed for all horizontal failure tests, as illustrated in Fig. 1A. Images from the optical high speed (HS) and infrared (IR) cameras during the failure event using an active cell at 30% SOC are shown in Figure 3. Two separate venting occurrences were observed, separated by around 4 minutes. The cell initially vented a small amount of fluid (likely gas and/or electrolyte), followed by a brief lull while the heater cell continued applying heat. Finally, the cell began vigorously smoking and ejecting fluid rapidly, although no fire, flame or sparks were generated likely as a result of the low SOC of the battery. Once the event had fully exhausted the battery contents, the heater cell was turned off and the assembly was allowed to cool slowly to room temperature while the chamber was safely vented of all hazardous gases.
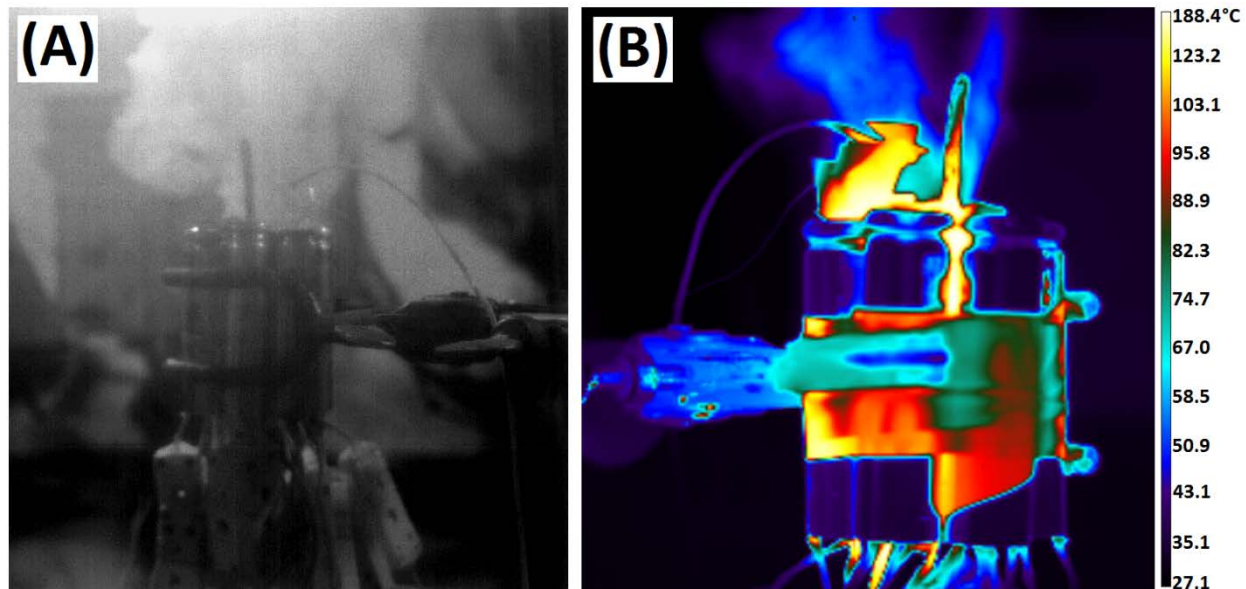
Figure 3. (A) High speed and (B) IR camera images for hex package 30% SOC failure test.

Figure 4 shows temperature vs. time data for the surrogate and 30% SOC active cells, as well as temperature differences for internal surrogate cell thermocouples. The maximum temperature at the top of the active cell was recorded to be 126°C (Fig. 4F) at the moment of the initial venting, at which point the thermocouple became detached from the package. Surrogate
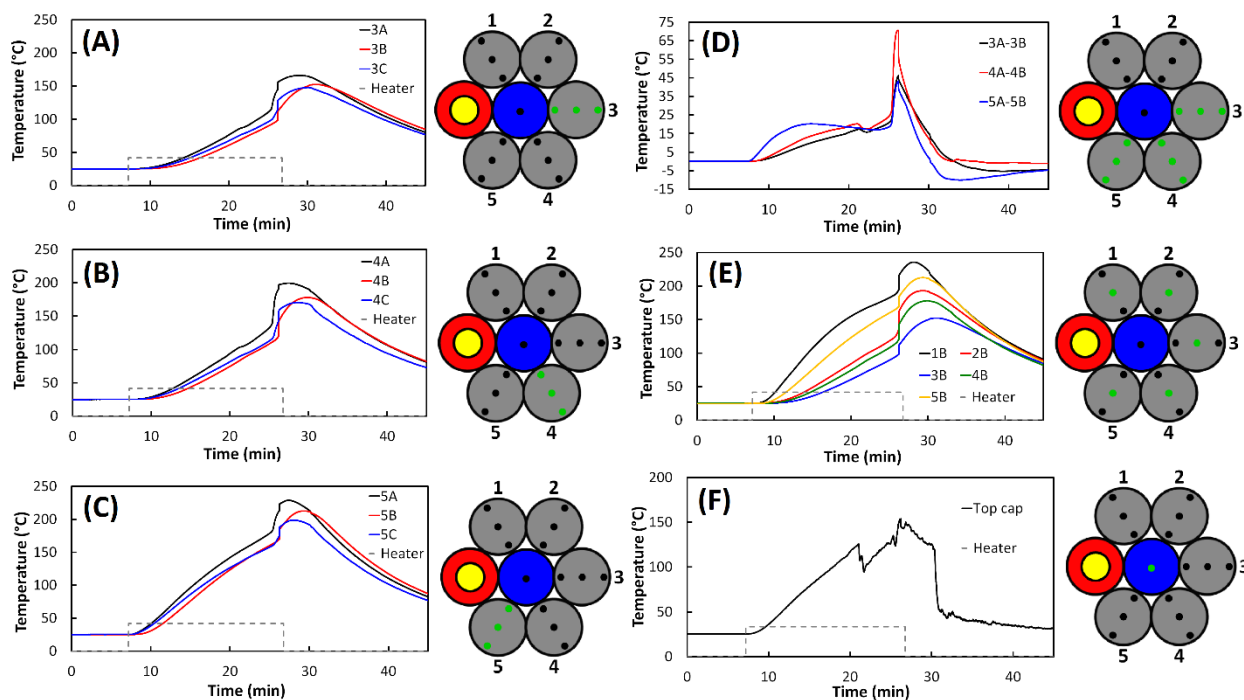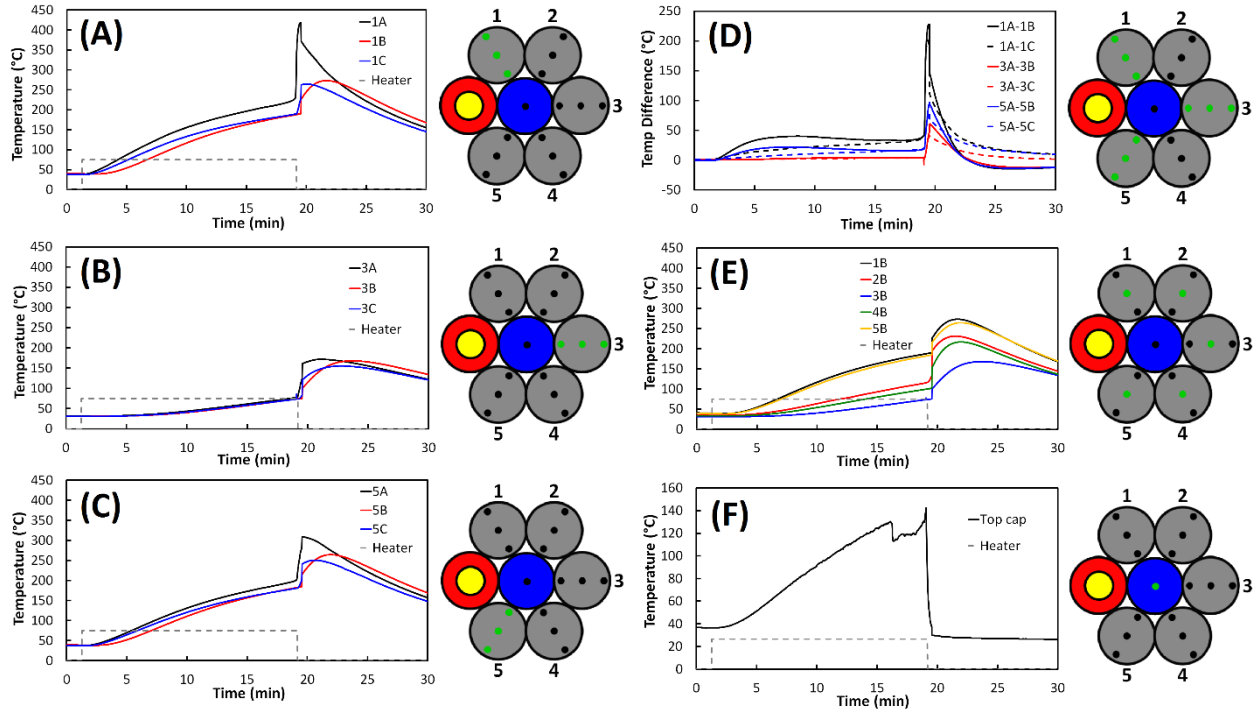

Figure 4. (A) through (C) show surrogate cell temperatures vs. time; (D) instantaneous internal temperature distributions; (E) 'B' position thermocouple temperatures vs. time; and (F) active cell top thermocouple temperature vs. time for hex package 30% SOC failure test.

5

cell internal temperatures reached maximum values of 148-236°C (Fig. 4A-C) during the final battery failure, illustrating the extreme capacity for energy transfer to adjacent cells during a single cell failure in a multi-cell pack, even at a low SOC. Instantaneous temperature differences reached as high as 46-71°C at the point of failure (Fig. 4D), demonstrating large internal temperature gradients which can cause hot spots and further battery failure in active cells. Finally, the largest temperatures were observed in surrogate cells 1 and 5 (Fig. 4E), which was expected since they were closest to the heater cell. During the initial heating stage, surrogate cells 1 and 5 received more heat due to direct contact with the heater cell than the other three surrogate cells. However, once the failure event began, all five surrogate cells experienced a similar degree of temperature rise from the heat expelled by the failing active cell since the contact was identical for all surrogate cells to the active cell. After several minutes of cooling, all five surrogate cells reached approximately the same temperature before returning to ambient conditions.

Hex package HS and IR camera images with a 100% SOC active cell are shown in Figure 5 with temperature-time graphs shown in Figure 6. Once again, two distinct events were observed: an initial venting occurred releasing a small amount of electrolyte, followed by a full failure around 2-3 minutes later. In this case, the failure event was much more energetic than the 30% SOC test and involved sparking before a long period of smoking. The active cell top cap thermocouple reached a maximum temperature of 130°C during the initial venting (Fig. 6F), and similarly to the 30% SOC test, slightly detached from the cell making temperature readings during the final failure event inaccurate. As expected, surrogate cells 1 and 5 again showed the highest temperatures among all surrogate cells (Fig. 6E) due to proximity to the heater cell, reaching 250-418°C maximum internal temperatures, compared to only 155-231°C maximum temperatures for surrogate cells 2, 3 and 4 (Fig. 6A-C). Instantaneous surrogate cell temperature differences shown in Fig. 6D were as large as 82-228°C for surrogate cells 1 and 5 during the failure event, and even reached 19-40°C during the heating period before failure. The greater output of energy during failure of the 100% SOC cell resulted in much greater internal temperature distributions than the 30% SOC cell. Additionally, during the failure event liquid was observed to bubble from the top of the active cell and drip down and around the other cells in the package. This liquid was likely not electrolyte considering the extremely high temperatures present inside the failing battery that caused vaporization, decomposition, or combustion of the electrolyte, but rather was probably
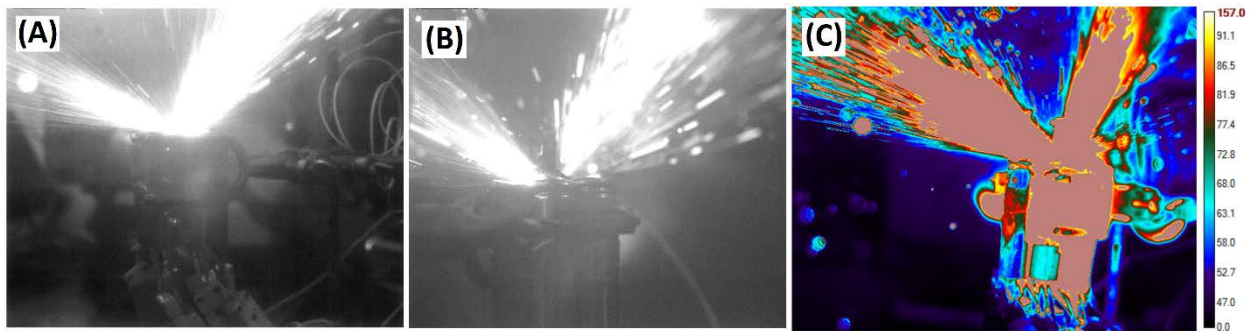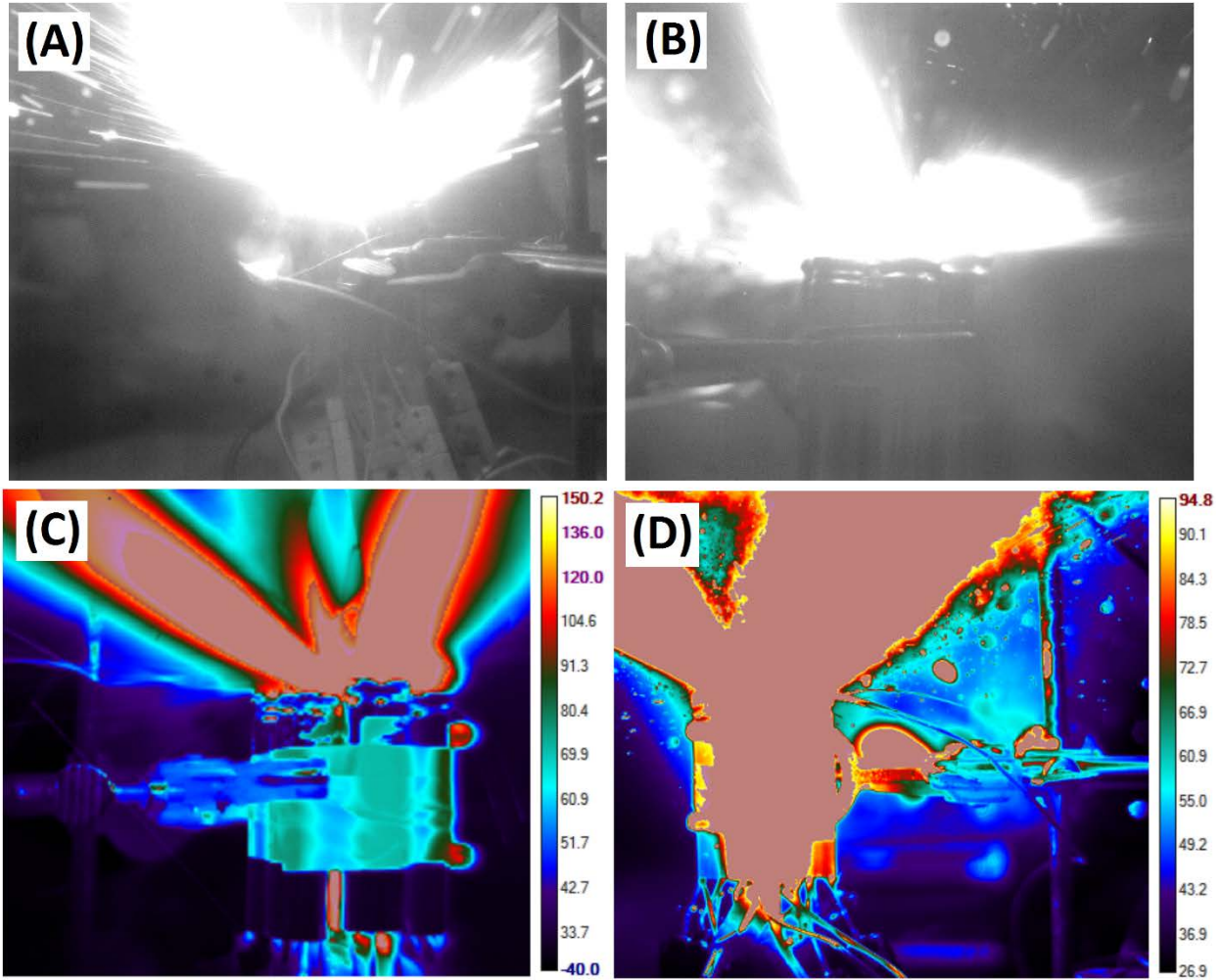

Figure 5. (A) and (B) show high speed camera images, and (C) shows IR camera images for hex package 100% SOC failure test.

6

Figure 6. (A) through (C) show surrogate cell temperatures vs. time; (D) instantaneous internal temperature distributions; (E) 'B' position thermocouple temperatures vs. time; and (F) active cell top thermocouple temperature vs. time for hex package 100% SOC failure test.

melted metals from the electrode materials (aluminum, copper, cobalt, and/or lithium) escaping and flowing out due to large internal pressures. This hot molten metal dripping around the active and surrogate cells may also have contributed to the extremely large temperatures seen in Fig. 6 compared with the 30% SOC test.

Figures 7 and 8 show HS and IR camera images, as well as temperature vs. time data, for the hex package with an overcharged-overheated active cell, respectively. In this test, the active cell was severely overcharged until the safety vent activated, causing the battery to permanently trip to open circuit. At this point, no current was able to be passed through the battery making pure overcharge failure an impossibility. For this reason, the heater cell was still used to bring the cell to the point of catastrophic failure. Similarly to the 100% SOC test, the overcharged battery produced a large amount of energy, sparking, and the force of the event caused the cell package to dislodge from the clamp holding it in place. The initial venting that took place when the battery was overcharged also resulted in the top thermocouple becoming detached, making accurate measurements of the top of the active cell during the ultimate failure event difficult. The maximum temperature observed from the top thermocouple on the active cell during the initial overcharge-induced venting was 141°C (Fig. 8F), and surrogate cell temperatures surprisingly only reached 114-259°C (Fig. 8A-C) during the failure event. These values were comparable to the 30% SOC test rather than the 100% SOC test, which was unexpected considering the greater level of stored energy and violence observed during the failure from the overcharged cell. It is possible

7

Figure 7. (A) and (B) show high speed camera and (C) and (D) IR camera images for overcharged hex package failure test.

that unlike the 100% SOC test, where hot molten liquid dripped around the cell package and inflated the temperature data, the majority of energy from the overcharged cell propagated vertically and in a very short time period such that the adjacent surrogate cells were not as heavily impacted. This short vertical burst may also be the reason that unlike the previous tests, there was not as dramatic a difference between surrogate cells 1 and 5 compared with the other three, save for the obvious spike observed with thermocouple 5B in Fig. 8E. The 30% SOC failure event, while less energetic, lasted longer during the period of smoking and venting which may explain why the overall maximum temperatures were close in magnitude. Finally, the explosive nature of the overcharged cell resulted in internal temperature distributions between 51-111°C (Fig. 8D) during failure, which were greater than the 30% SOC test results.
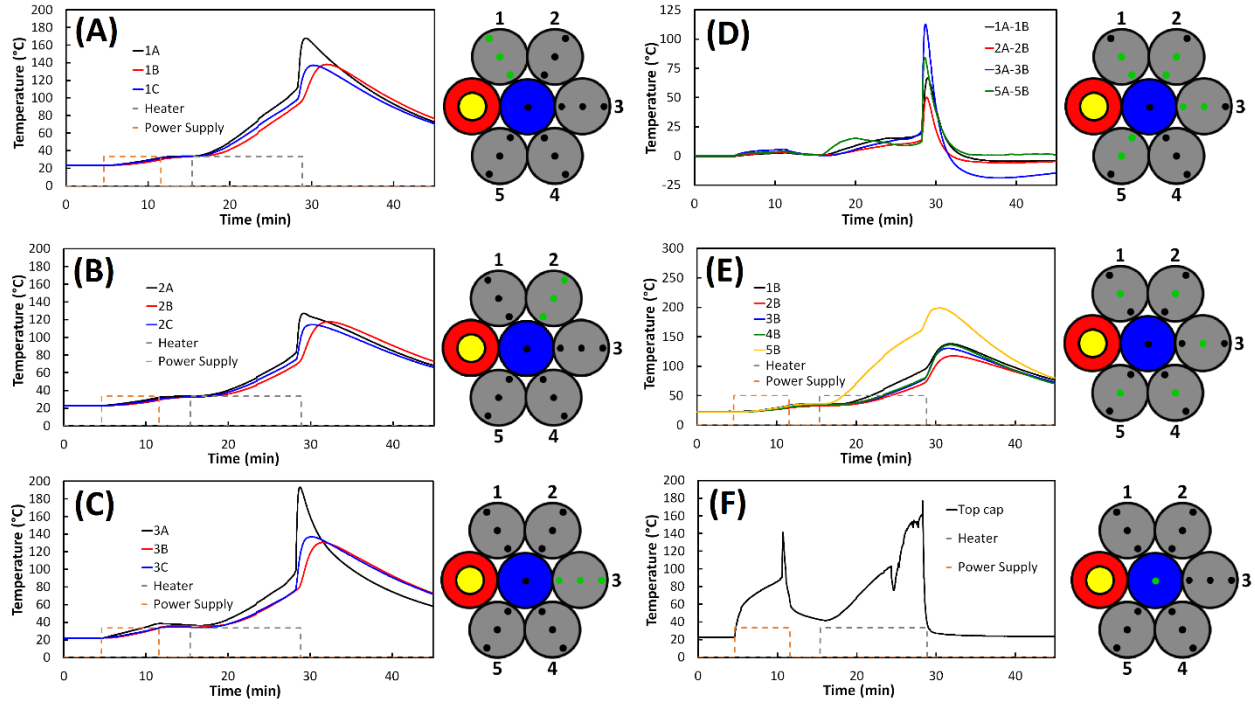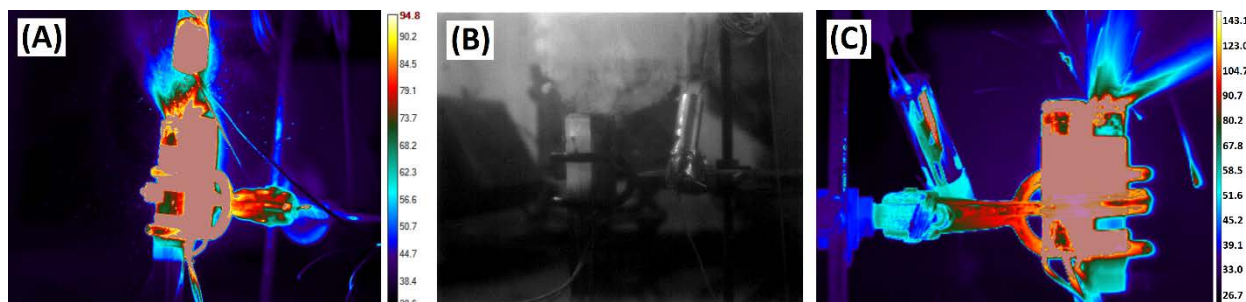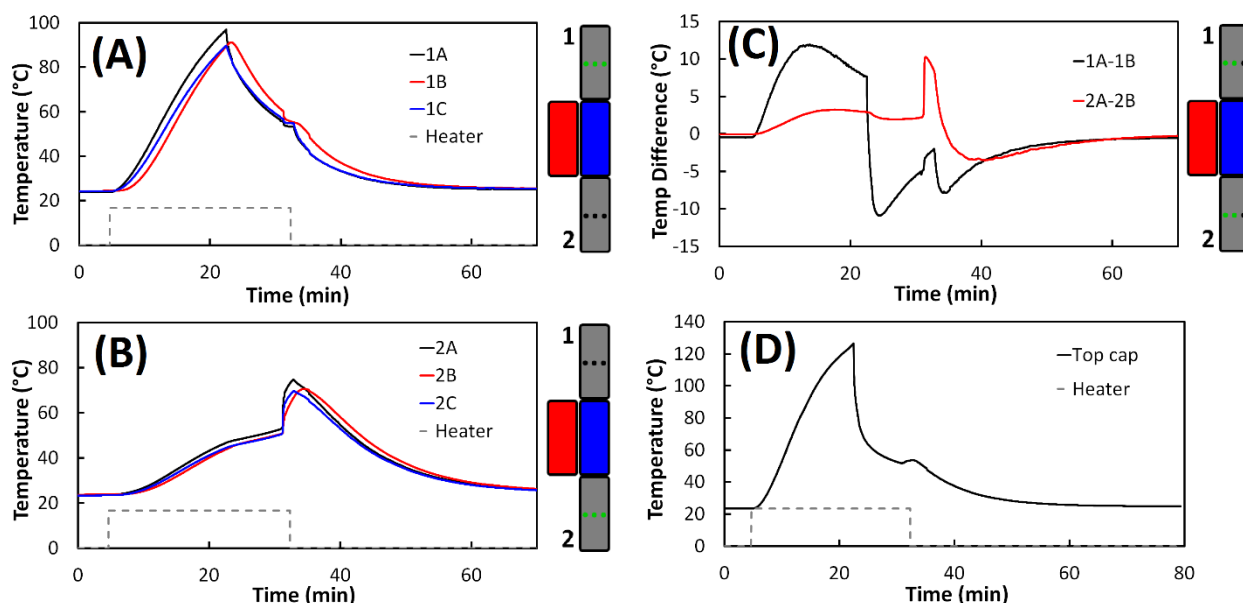
Figure 8. (A) through (C) show surrogate cell temperatures vs. time; (D) instantaneous internal temperature distributions; (E) 'B' position thermocouple temperatures vs. time; and (F) active cell top thermocouple temperature vs. time for overcharged hex package failure test.

3.2 Vertical Packing

For the vertical failure tests, a separate cell arrangement was created, which is shown in Fig. 1B. Three different SOCs (30%, 100% and overcharged) were again applied for the vertical arrangement of cells. Figure 9 shows the HS and IR camera images for the 30% SOC test, and Figure 10 shows accompanying temperature vs. time graphs. The failure observed for the 30% SOC vertical test was similar to the 30% hex package test, with an initial venting followed (after around 8-9 minutes) by complete failure with vigorous smoking but no flames or sparking. During the initial venting, the rapid release of fluid from the top of the active cell caused the top surrogate cell to be ejected from the package, as evident in the images shown in Fig. 9. The top thermocouple also became dislodged at that time, giving an indication of the temperature of vented material only during the initial safety vent trigger. The maximum top thermocouple temperature was 127°C (Fig. 10D), and the top surrogate cell reached 90-97°C (Fig. 10A) during this initial venting before being removed from the cell package. During the final failure event, the bottom surrogate cell only reached 70-75°C, further illustrating that heat propagated mostly in the vertical direction at the point where materials were ejected. Finally, the maximum internal temperature distributions observed in both surrogate cells was only 3-12°C, which was expected considering the previously-mentioned anisotropy in thermal conductivity between axial and radial energy flow. Since nearly all heat propagated axially in the vertical package tests, and all surrogate cell internal thermocouples were equidistant axially from the active cell, very little temperature distribution was expected.
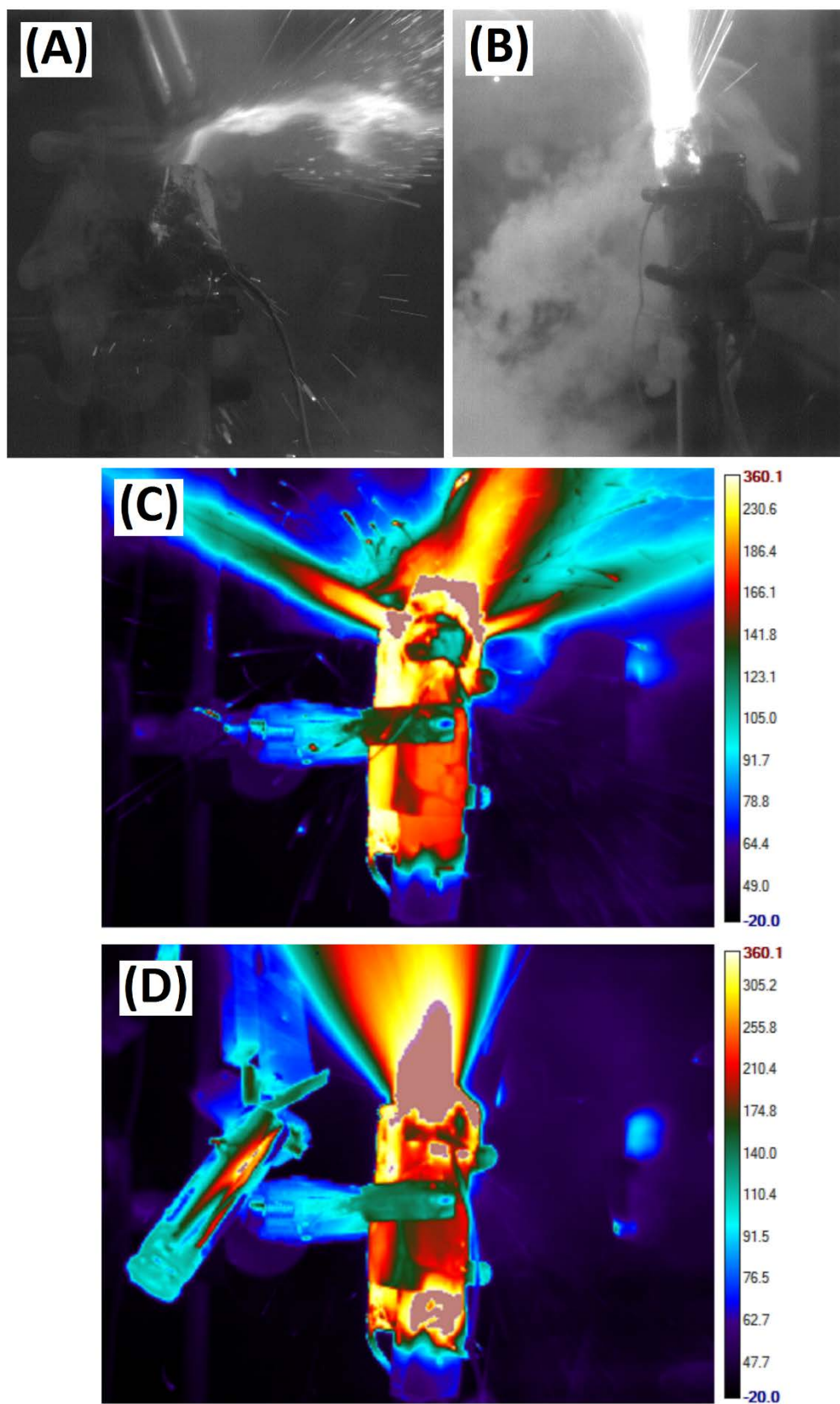
9

Figure 9. High speed and IR camera images for vertical package 30% SOC test.
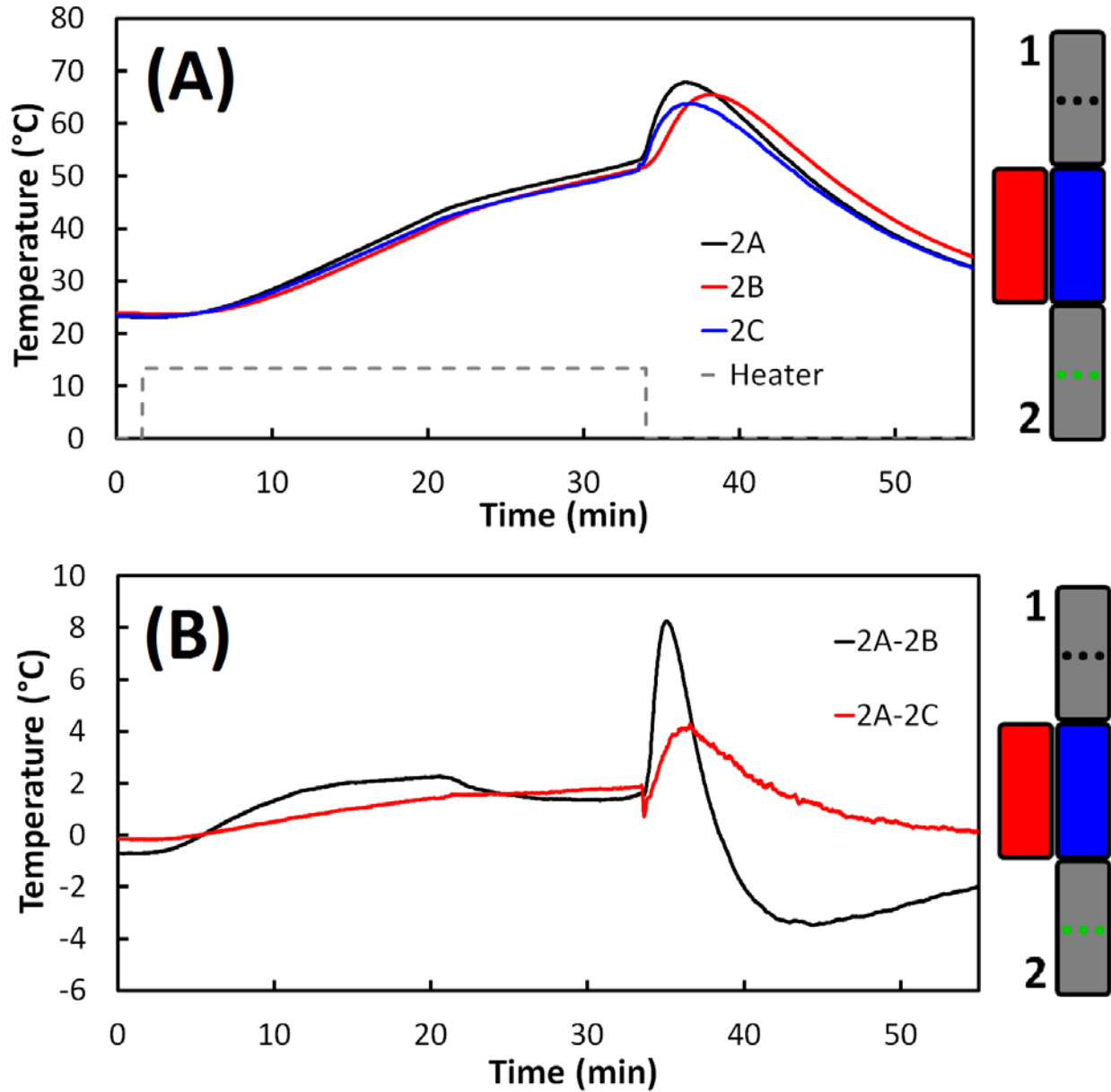

Figure 10. (A) and (B) show surrogate cell temperatures vs. time; (C) shows instantaneous internal temperature distributions; and (D) shows active cell top thermocouple temperatures vs. time for vertical package 30% SOC test.

Figures 11 and 12 show camera images and temperature-time data for the 100% SOC vertical package test, respectively. Similar behavior was observed compared with the hex package test for a 100% SOC active cell: an initial venting occurred (which did not eject the top surrogate cell from the package), followed after around 13-14 minutes by the ultimate failure event where sparks, fire and ejected materials were observed. During this event, the top surrogate cell was finally ejected away from the cell package, and in the process both the top surrogate cell and top thermocouple became severely damaged, leading to a loss of data for those elements. Much like the 30% SOC test, bottom surrogate cell internal temperatures were not very high, peaking at only 64-68°C (Fig. 12A), and internal temperature distributions in surrogate cell 2 were only 4-8°C (Fig. 12B), further illustrating the anisotropy of the 18650 cells.

Overcharged and overheated HS and IR camera failure images for the vertical package are shown in Figure 13, along with temperature vs. time data in Figure 14. Overcharging the cell again caused a safety vent to trigger, sending the battery to open circuit. In this case, the initial
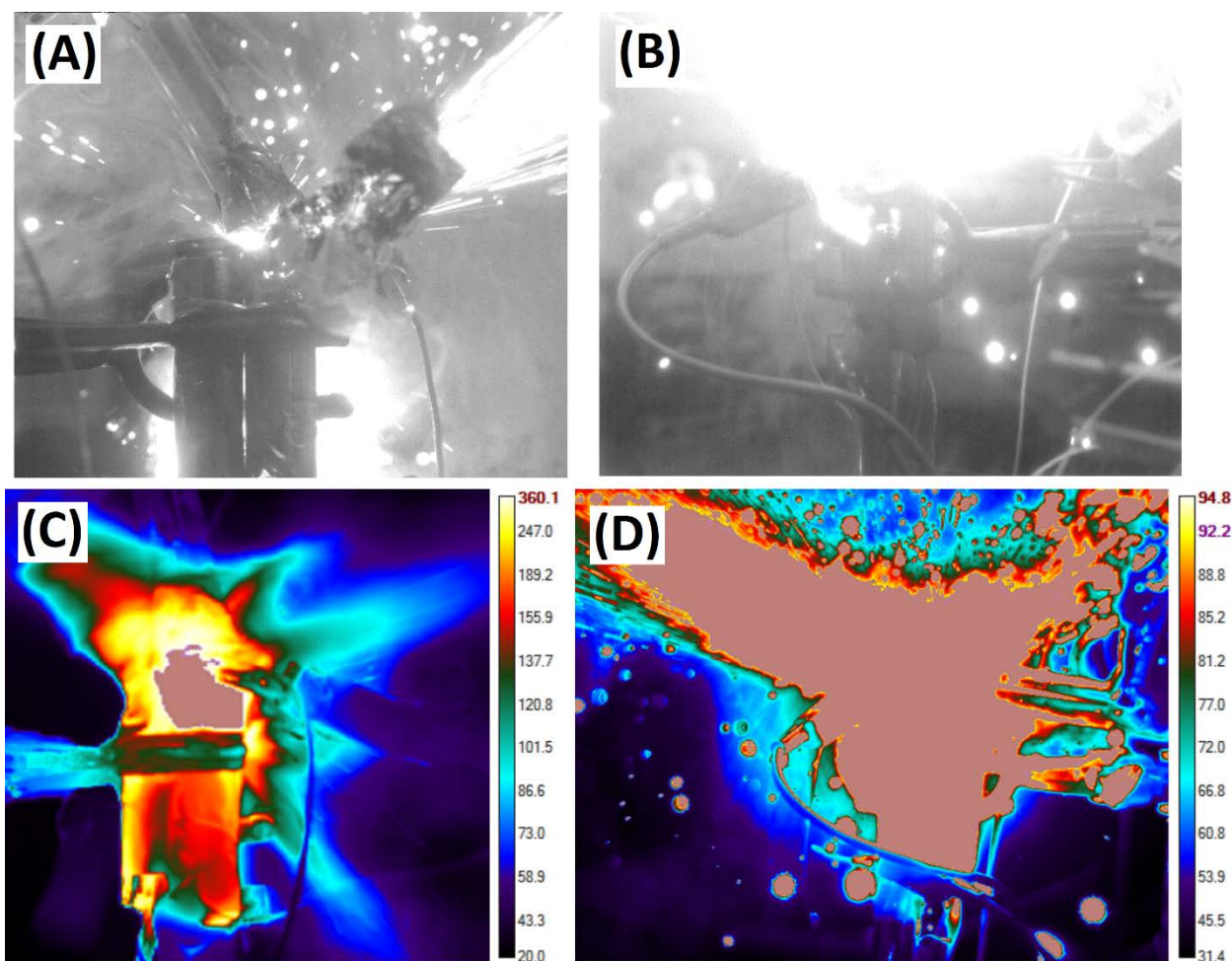
Figure 11. High speed and IR camera images for vertical package 100% SOC test.

Figure 12. (A) surrogate cell temperatures vs. time, and (B) instantaneous internal temperature distributions for vertical package 100% SOC test.

overcharge venting fortunately did not cause either the top surrogate cell or top thermocouple to dislodge, allowing measurements to be made throughout the experiment. The maximum top thermocouple temperature during the initial venting was 107°C, and there was only a negligible rise in surrogate cell temperature before the heater cell was turned on. During the catastrophic failure event, the top thermocouple reached a staggering maximum temperature of 805°C (Fig. 14D), and the top surrogate cell registered 91-109°C (Fig. 14A) before it was ultimately ejected from the package during the intense sparking, flames, and fluids being spewed from the active cell during failure. The bottom surrogate cell reached 89-96°C (Fig. 14B) which was higher than the previous two vertical package tests and was likely a result of a much greater energy output during

Figure 13. High speed and IR camera images for overcharged vertical package test.

failure due to overcharged conditions. Despite the increased energy output, however, a maximum internal temperature distribution of just 8-19°C was seen (Fig. 14C), consistent with all vertical package tests performed in this study.

Vertical package tests showed only a modest level of internal temperature rise in all surrogate cells compared with the hex package tests. Due to the propagation of energy during failure being primarily in the vertical direction, this result was surprising at first; however, considering that the top surrogate cell was ejected from the package during all three vertical package tests, it was not able to be in the direct stream of energy flow for the entire duration of failure in any test. Also, for the hex package tests there were more cells present, causing a larger mass, greater overall heat capacity for the package, and a degree of insulation for all cells involved that likely led to higher heat retention and larger recorded temperatures. However, in a real large format battery pack, there are typically numerous cells situated in close proximity, and these results suggest that while being horizontally-located near a failing cell is certainly dangerous and problematic, any cells placed above a failing battery will likely be at higher levels of risk for coming into contact with heat, fire, sparks, and hazardous ejected materials.

13
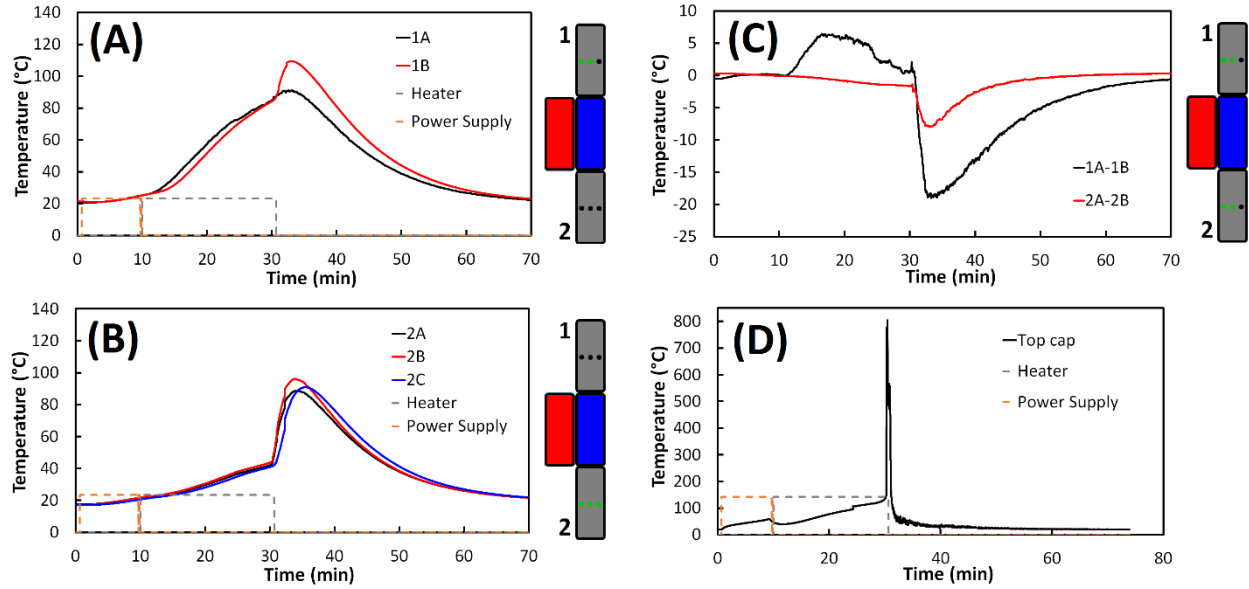
Figure 14. (A) and (B) show surrogate cell temperatures vs. time; (C) shows instantaneous internal temperature distributions vs. times; and (D) shows active cell top thermocouple temperature vs. time for overcharged vertical package test.

4.0 Summary & Conclusions

A series of failure experiments were conducted using $LiCoO_2$ 18650 lithium-ion batteries and custom-designed and fabricated 18650 surrogate cells. Two parameters were varied: active cell state of charge and cell packing configuration. Three different states of charge were applied (30%, 100%, and overcharged) and two different packing configurations were constructed and tested (horizontal/hexagonal package and vertical package). Batteries were induced to failure using an adjacent cartridge heater embedded inside an 18650 cell casing to act as a heat source. Higher states of charge resulted in much more energetic failure events and generally led to higher temperatures. For the hex package tests, surrogate cells closest to the heater cell experienced the greatest temperature rise, and all surrogate cells had internal temperature spikes during the active cell failure event. Internal temperature distributions were extremely large during the heating period and failure events for all hex package tests, but not for vertical package tests, as a result of the anisotropy in radial and axial thermal conductivity of 18650 cells. These results illustrate the effectiveness of the custom surrogate cells for determining internal battery temperatures during a catastrophic failure event without the need of multiple active cells, and also of the dangers associated with battery failure in a multi-cell pack in both the radial and axial directions.

14

5.0 References

1.   S. Rose-Pehrsson, M. Hammond, B. Williams, J. Fleming, R. Sheinson, F. Williams, D. Fuentevilla, C. S. Winchester, N. Begue and C. Field, "The products produced from individual cells which comprise a large lithium oxyhalide battery when thermally abused." *NRL Letter Report* 6180/0315A, 3 December 2009.

2.   S. Rose-Pehrsson, M. Hammond, B. Williams, J. Fleming, R. Sheinson, F. Williams, D. Fuentevilla, C. S. Winchester, N. Begue and C. Field, "The products produced from individual cells which comprise a large lithium oxyhalide battery when thermally abused-series 2." *NRL Letter Report* 6104/0003, 29 March 2010.

3.   S. Rose-Pehrsson, M. Hammond, B. Williams, J. Fleming, R. Sheinson, F. Williams, D. Fuentevilla, N. Begue and C. Field, "The products produced from lithium ion battery when thermally abused." *NRL Letter Report* 6104/0004, 2 April 2010.

4.   G. G. Back, C. S. Winchester and F. W. Williams, "Lithium battery fire test data summary report." *NRL Letter Report* 6104/0003, 11 November 2012.

5.   F. Williams, S. Rose-Pehrsson, B. Williams, J. Fleming, E. Fallows, N. Begue, C. Field and K. Myers, "The products produced during thermal abuse from assorted generic lithium batteries associated with technology insertion program (TIPS)." *NRL Letter Report* 6104/0010, 29 September 2010.

6.   F. W. Williams, G. G. Back, A. F. Durkin, H. V. Pham, X. Nguyen and C. S. Winchester, "Joint strike fighter/USMC saber improved target acquisition system lithium-ion battery casualty hazard mitigation suite validation test results." *NRL Letter Report* 6104/0010, 31 October 2011.

7.   F. W. Williams, A. F. Durkin, C. S. Winchester and H. V. Pham, "Tests to support development of a lithium battery casualty mitigation system (LBCMS) - phase 1: heat release rate baseline data." *NRL Letter Report* 6104/0017, 13 September 2010.

8.   G. G. Back, A. F. Durkin, X. Nguyen, H. V. Pham, S. Duncan, C. S. Winchester, J. Gratz and F. W. Williams, "Lithium battery casualty mitigation system (LBCMS) development tests – brass board tests (quick look)." *NRL Letter Report* 6104/0009, 5 July 2011.

9.   F. W. Williams, H. V. Pham, A. F. Durkin, C. S. Winchester and G. G. Back, "Lithium battery casualty mitigation system (LBCMS) – brass board test results." *NRL Letter Report* 6104/0015, 14 November 2011.

10.   F. W. Williams and S. L. Rose-Pehrsson, "A test plan for the tips program to measure the gaseous species production of generic lithium batteries exposed to thermal abuse." *NRL Letter Report* 6104/0005, 19 April 2010.

11. G. G. Back, J. Williamson and F. W. Williams, "Lithium battery casualty mitigation system (LBCMS) development – potential gas production caused by electrolysis." *NRL Letter Report* 6104/0015, 9 July 2010.

12. C. R. Field, S. Tuttle, B. Williams, J. Fleming, J. Farley, S. Rose-Pehrsson, F. Williams, M. Huffman and C. Winchester, "A test plan for the evaluation of lithium ion battery cell failure propagation." *NRL Letter Report* 6180/0118A, 5 July 2012.

13. C. R. Field, B. A. Williams, T. Kummerer, J. Fleming, S. Rose-Pehrsson, D. Fuentevilla and K. Myers, "The products produced from individual cells which comprise a large lithium iron phosphate battery when thermally abused." *NRL Letter Report* 6180/0236A, 23 October 2011.

14. C. R. Field, S. Rose-Pehrsson, D. Fuentevilla and K. Myers, "The products produced from worst-case scenario testing of large lithium iron phosphate battery failure inside a quadruple container (quadcon)." *NRL Letter Report* 6180/0243A, 23 October 2011.

15. F. W. Williams and G. G. Back, "Lithium battery fire tests and mitigation." *NRL Formal Report* NRL/FR/6104-14-10,262, 25 August 2014.

16. C. R. Field, M. H. Hammond, S. G. Tuttle, B. A. Williams, S. L. Rose-Pehrsson, N. S. Spinner, K. M. Myers and A. L. Lubrano, "Demonstration of experimental infrastructure for studying cell-to-cell failure propagation in lithium-ion batteries." *NRL Memorandum Report* NRL/MR/6180-14-9563, 11 September 2014.

17. N. S Spinner, R. Ananth, S. G. Tuttle, S. L. Rose-Pehrsson, R. Mazurick and A. Brandon, "Lithium battery safety/cell-to-cell failure project FY14 progress report." *NRL Memorandum Report* NRL/MR/6180-15-9601, 6 March 2015.

18. N. S. Spinner, C. R. Field, M. H. Hammond, B. A. Williams, K. M. Myers, A. L. Lubrano, S. L. Rose-Pehrsson and S. G. Tuttle, "Physical and chemical analysis of lithium-ion battery cell-to-cell failure events inside custom fire chamber." *J. Power Sources* **279** (2015) 713-721.

19. T. B. Bandhauer, S. Garimella and T. F. Fuller, "A critical review of thermal issues in lithium-ion batteries." *J. Electrochem. Soc.* **158** (2011) R1-R25.

20. Y. Fu, S. Lu, K. Li, C. Liu, X. Cheng and H. Zhang, "An experimental study on burning behaviors of 18650 lithium ion batteries using a cone calorimeter." *J. Power Sources* **273** (2015) 216-222.

21. F. Larsson and B.-E. Mellander, "Abuse by external heating, overcharge and short circuiting of commercial lithium-ion battery cells." *J. Electrochem. Soc.* **161** (2014) A1611-A1617.

22. X. Liu, S. I. Stoliarov, M. Denlinger, A. Masias and K. Snyder, "Comprehensive calorimetry of the thermally-induced failure of a lithium ion battery." *J. Power Sources* **280** (2015) 516-525.

23. N. S. Spinner, R. Mazurick, A. Brandon, S. L. Rose-Pehrsson and S. G. Tuttle, "Analytical, numerical and experimental determination of thermophysical properties of commercial 18650 $LiCoO_2$ lithium-ion battery." *J. Electrochem. Soc.* **162** (2015) A2789-2795.

24. S. J. Drake, D. A. Wetz, J. K. Ostanek, S. P. Miller, J. M. Heinzel and A. Jain, "Measurement of anisotropic thermophysical properties of cylindrical Li-ion cells." *J. Power Sources* **252** (2014) 298-304.

25. H. Maleki, S. Al Hallaj, J. R. Selman, R. B. Dinwiddie and H. Wang, "Thermal properties of lithium-ion battery and components." *J. Electrochem. Soc.* **146** (1999) 947-954.

26. G. Zhang, L. Cao, S. Ge, C.-Y. Wang, C. E. Shaffer and C. D. Rahn, "In situ measurement of radial temperature distributions in cylindrical Li-ion cells." *J. Electrochem. Soc.* **161** (2014) A1499-A1507.

27. R. Srinivasan and B. G. Carkhuff, "Empirical analysis of contributing factors to heating in lithium-ion cells: anode entropy versus internal resistance." *J. Power Sources* **241** (2013) 560-566.

28. R. A. Leising, M. J. Palazzo, E. S. Takeuchi and K. J. Takeuchi, "Abuse testing of lithium-ion batteries: characterization of the overcharge reaction of $LiCoO_2$/graphite cells." *J. Electrochem. Soc.* **148** (2001) A838-A844.

29. D. Belov and M.-H. Yang, "Investigation of the kinetic mechanism in overcharge process for Li-ion battery." *Solid State Ionics* **179** (2008) 1816-1821.

30. N. S. Spinner, K. M. Hinnant, R. Mazurick, A. Brandon, S. L. Rose-Pehrsson and S. G. Tuttle, "Novel 18650 lithium-ion battery surrogate cell design with anisotropic thermophysical properties for studying failure events." *J. Power Sources* Submitted.